

Mass and energy balance calculations for an artificial ice reservoir (Icestupa)

Suryanarayanan Balasubramanian^{1,*}, Martin Hoelzle¹, Michael Lehning²,

Sonam Wangchuk³, Johannes Oerlemans⁴ and Felix Keller⁵

¹ University of Fribourg, Fribourg, Switzerland

² WSL Institute for Snow and Avalanche Research, Davos, Switzerland

³ Himalayan Institute of Alternatives Ladakh, Leh, India

⁴ Institute for Marine and Atmospheric Research, Utrecht University, Utrecht, The Netherlands

⁵ Academia Engiadina, Samedan, Switzerland

Correspondence*:

Suryanarayanan Balasubramanian

suryanarayanan.balasubramanian@unifr.ch

2 ABSTRACT

Artificial Ice Reservoirs (AIRs) have been successful in storing water during winter and releasing the water during spring and summer. This has made them a reliable fresh water resource for irrigation in dry environments. Several AIRs have been built but studies of their water storage capacity and efficiency are scarce. This study attempts to model a cone-shaped AIR popularly called Icestupa. Important processes involved in the development and temporal evolution of an Icestupa are calculated by a physically-based model using equations governing the heat transfer, vapour diffusion and transport of water that undergoes phase changes. These processes were quantified using meteorological data in conjunction with fountain spray information (mass input of an Icestupa) to estimate the quantity of frozen, melted, evaporated and runoff water at a location called 'Eispalast' in Fribourg, Switzerland. At this measurement site, an Icestupa was built for model validation purposes. The model was further tested by performing sensitivity and uncertainty study showing that the most sensitive parameters are the ice emissivity and the temperature threshold used to determine precipitation phase. Model calculations estimate that the Eispalast Icestupa stored about 8% of the total water sprayed as ice. In addition, we found that reducing nozzle diameter of the fountain from 5 mm to 3 mm increases the storage efficiency up to 93% without compromising on the storage duration.

Keywords: iceslupa, mass balance, water storage, climate change adaptation, geoengineering

1 INTRODUCTION

Seasonal snow cover, glaciers and permafrost are expected to change their water storage capacity due to climate change with major consequences for downriver water supply (Immerzeel et al., 2019). The challenges brought about by these changes are especially important for dry mountain environments such as in Central Asia or the Andes, which directly rely on the seasonal meltwater for their farming and drinking needs (Hoelzle et al., 2019; Apel et al., 2018; Buytaert et al., 2017; Chen et al., 2016; Unger-Shayesteh



Figure 1. Icestupa in Ladakh, India on March 2017 was 24 m tall and contained around 3700 m^3 of water. Picture Credits: Lobzang Dadul

25 et al., 2013). Some villages in Ladakh, India have already been forced to relocate due to glacial retreat and
26 the corresponding loss of their main fresh water resources (Grossman, 2015).

27 AIRs have been considered to be a feasible way to adapt to these changes (Hock et al., 2019; Nüsser
28 et al., 2019b). An artificial ice reservoir is a human-made ice structure typically constructed during the
29 cold winter months and designed to slowly release freshwater during the warm and dry spring and summer
30 months. The main purpose of AIRs is irrigation. Therefore, AIRs are designed to store water in the form of
31 ice as long into the summer as possible. The energy required to construct an AIR is usually derived from
32 the gravitational head of the source water body. Some are constructed horizontally by freezing water using
33 a series of checkdams and others are built vertically by spraying water through fountain systems (Nüsser
34 et al., 2019a). The latter are colloquially referred to as Icestupas and are the subject of this study.

35 A typical Icestupa just requires a pipeline attached to a vertically mounted metal pipe with a fountain
36 nozzle for construction. Water source is usually a high altitude lake or glacial stream. Due to the altitude
37 difference between the pipeline input and fountain output, water ejects from the fountain nozzle as droplets
38 that eventually lose their latent heat to the atmosphere and accumulate as ice around the metal pipe.
39 The fountain nozzle is raised through addition of further pipes as and when significant ice accumulates.
40 Typically, a dome of branches is constructed around the metal pipe so that such pipe extensions can be
41 done from within this dome. During the winter, the fountain is manually activated between sunset and
42 sunrise. Threads, tree branches and fishing nets are used to guide and accelerate the ice formation.

43 Since their invention in 2013 (Wangchuk, 2014), Icestupas have gained widespread publicity in the region
44 of Ladakh, Northern India since they require very little infrastructure, skills and energy to be constructed
45 in comparison to other water storage technologies. Compared to other AIR geometries, Icestupas (Fig.
46 1) can be built at lower altitudes and last much longer into the summer than other types of ice structures
47 (Wangchuk, 2014). However, to date, no reliable estimates exist about the amount of sprayed water that
48 is necessary to create them and the meltwater they provide (Nüsser et al., 2019a). Rough estimates of
49 Icestupa meltwater in Ladakh suggest that the water loss during the construction process is considerable
50 (see Appendix 8.1). A complete set of measurements of the water storage and energy balance are required
51 to understand the cause of the water losses better and increase the construction efficiency.

In this paper, we aim to develop a physically-based model of a vertical AIR (or Icestupa) that can quantify their storage efficiency using existing weather and water usage information. Mass and energy balance equations were used to estimate the quantity of water frozen, melted, evaporated and runoff. Sensitivity and uncertainty analysis were performed to identify the most critical parameters and the variance caused by them. For validation, we created an Icestupa at an accessible site (called Eispalast) near Schwarzsee in the Canton of Fribourg, Switzerland, allowing easy maintenance and control of the measurements. Due to the low altitude of the site with relatively high winter temperatures, only a small Icestupa could be established during winter 2018/19 for providing us with model validation data. Our model and validation experiments provide first steps towards evaluating the effectiveness of a vertical AIR for irrigation and finally we outline some preliminary guidelines for consideration when a construction of an Icestupa for water storage is envisaged.

2 STUDY SITE

The Eispalast (EP) site in the Schwarzsee region lies at 967 m a.s.l.. In the winter (Oct-Apr), mean daily maximum and minimum air temperatures vary between 14 to -4 °C. Clear skies are rare, averaging around 7 days, and precipitation amounts average 155 mm per month during winter (Meteoblue, 2020). The site was situated adjacent to a stream resulting in high humidity values across the study period. Within the Eispalast site, 1.8 m in radius enclosure was constructed for the experiment. An automatic weather station (AWS) was set in place adjacent to the wooden boundary as shown in Fig. 2. The fountain used for spraying water had a nozzle diameter of 5 mm and a height of 1.35 m, and was placed in the centre of the wooden enclosure. The water was transferred from a spring water source at 1267 m a.s.l. by pipeline and flowed via a flowmeter and an air escape valve to the nozzle, where it was sprinkled with a spray radius of around 1.7 m. The air escape valve was installed to avoid errors in the flow measurements due to air bubbles. In addition, a webcam guaranteed a continuous survey of the site during the construction of the Icestupa.

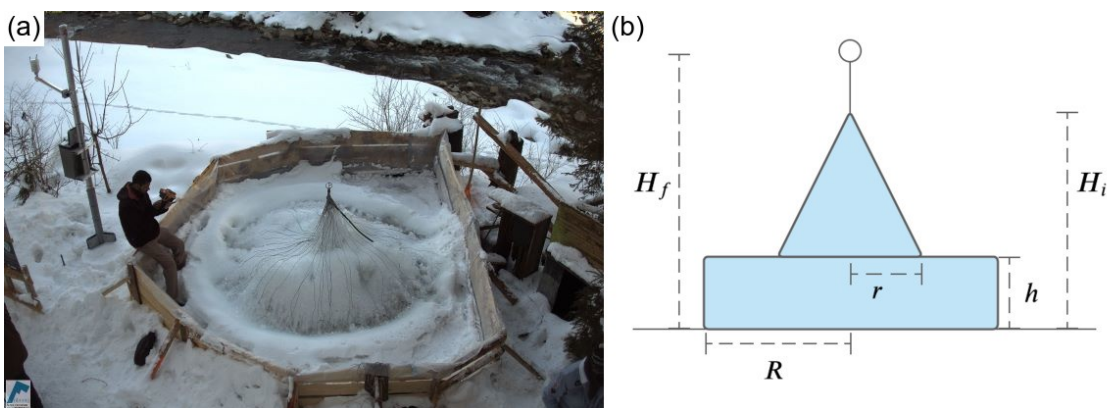


Figure 2. (a) The ice structure during the first validation measurement as seen on the webcam image of 14th Feb. (b) The corresponding cross section of the EP ice structure with the field estimates of r , R , h , H_i , H_f used to determine the Icestupa volume is shown on the right.

2.1 Construction

From 30th January to 18th March 2019 the Icestupa was constructed through the fountain spray, which was manually switched on if measured air temperature was below -5 °C after sunset and was switched off as soon as the ice was exposed to daylight or temperatures were above 0 °C. The water spray of the fountain was initially adjusted so that most of the water droplets land within the wooden boundary zone. The ice formation was guided by adding a metal framework at the ice structure base after the first night of

80 operation. Several cotton threads were tied between the ice structure base and fountain pole for accelerating
81 and further guiding the ice formation process.

82 2.2 Measurements and Data

83 The EP AWS was located at 967 m a.s.l. It was in operation from 30th January to 18th March 2019.
84 Measurements comprise air temperature, relative humidity, water flow rate, wind speed and direction. All
85 these measurements were stored at a 5 minute sample rate. The water flow rate or discharge was measured
86 via an ultrasonic sensor attached to the fountain supply pipeline. Precipitation data was derived from the
87 Plaffeien AWS (IDAWEB, 2019) located 8.8 km away from the measurement site at an altitude of 1042 m
88 a.s.l.

89 ERA5 reanalysis dataset (Copernicus Climate Change Service (C3S), 2017) correlates much better to
90 lower elevation sites in Switzerland (Scherrer, 2020). Moreover, all the EP meteorological parameters
91 except precipitation correlated better with ERA5 dataset compared to the nearby Plaffein AWS. Namely,
92 the 2 m temperature parameter correlated ($r^2 = 0.9$) with air temperature, surface pressure parameter
93 correlated ($r^2 = 1$) with air pressure and 10m wind speed parameter (derived from horizontal and vertical
94 components) correlated ($r^2 = 0.6$) with wind speed. Direct and diffuse shortwave radiation were also
95 derived from ERA5 surface solar radiation downwards and total sky direct solar radiation parameter. The
96 hourly ERA5 data and the 10 minute Plaffeien AWS data were linearly interpolated to the 5 minute data
97 frequency of the EP AWS.

98 Due to a power failure, all data from the EP AWS was lost between 27th February 15:20 2019 to 2nd
99 March 15:00 2019. Consequently, the amount of missing data in the dataset was around 7%. During heavy
100 snowfall events, the ultrasonic wind sensor was blocked and recorded zero values. ERA5 was used to
101 fill such errors and data gaps . Near-surface humidity is not archived directly in ERA datasets, but from
102 near-surface (2 m from the surface) temperature (T_{ERA5}) and dew point temperature (Tw_{ERA5}) one can
103 calculate relative humidity(RH) at 2 m as follows:

$$RH = 100 \cdot \frac{e_{sat}(Tw_{ERA5})}{e_{sat}(T_{ERA5})} \quad (1)$$

104 where the saturation vapour pressure function e_{sat} is expressed with the Teten's formula (Tetens, 1930):

$$e_{sat}(T) = a_1 \cdot e^{(a_3 \cdot \frac{T}{T+273.16-a_4})} \quad (2)$$

105 with T in °C and the parameters set for saturation over water ($a_1 = 611.21$ Pa, $a_3 = 17.502$ and $a_4 = 32.19$
106 K) according to Buck (1981). Zero wind speed values were recorded whenever snow accumulated on the
107 ultrasonic wind sensor. So all null values were replaced using the ERA5 dataset.

108 The ERA5 grid point chosen (Latitude 46° 38' 24" N, Longitude 7° 14' 24" E) for the EP site was around
109 9 km away from the actual site. So all the ERA5 variables were fitted with the Schwarzee dataset via linear
110 regressions. Through this modified ERA5 dataset, we were also able to further extend the EP dataset and
111 allow the model to run beyond 18th March 2019. Precipitation was filled as null values beyond 18th March
112 2019.

113 2.2.1 Field Measurements for validation

114 The volume was determined by decomposing the ice structure into a cylinder (length $2R$ and height h)
115 and a cone (radius r and height ($H_i - h$)) through the following equation:

$$V = \pi \cdot R^2 \cdot h + 1/3 \cdot \pi \cdot r^2 \cdot (H_i - h) \quad (3)$$

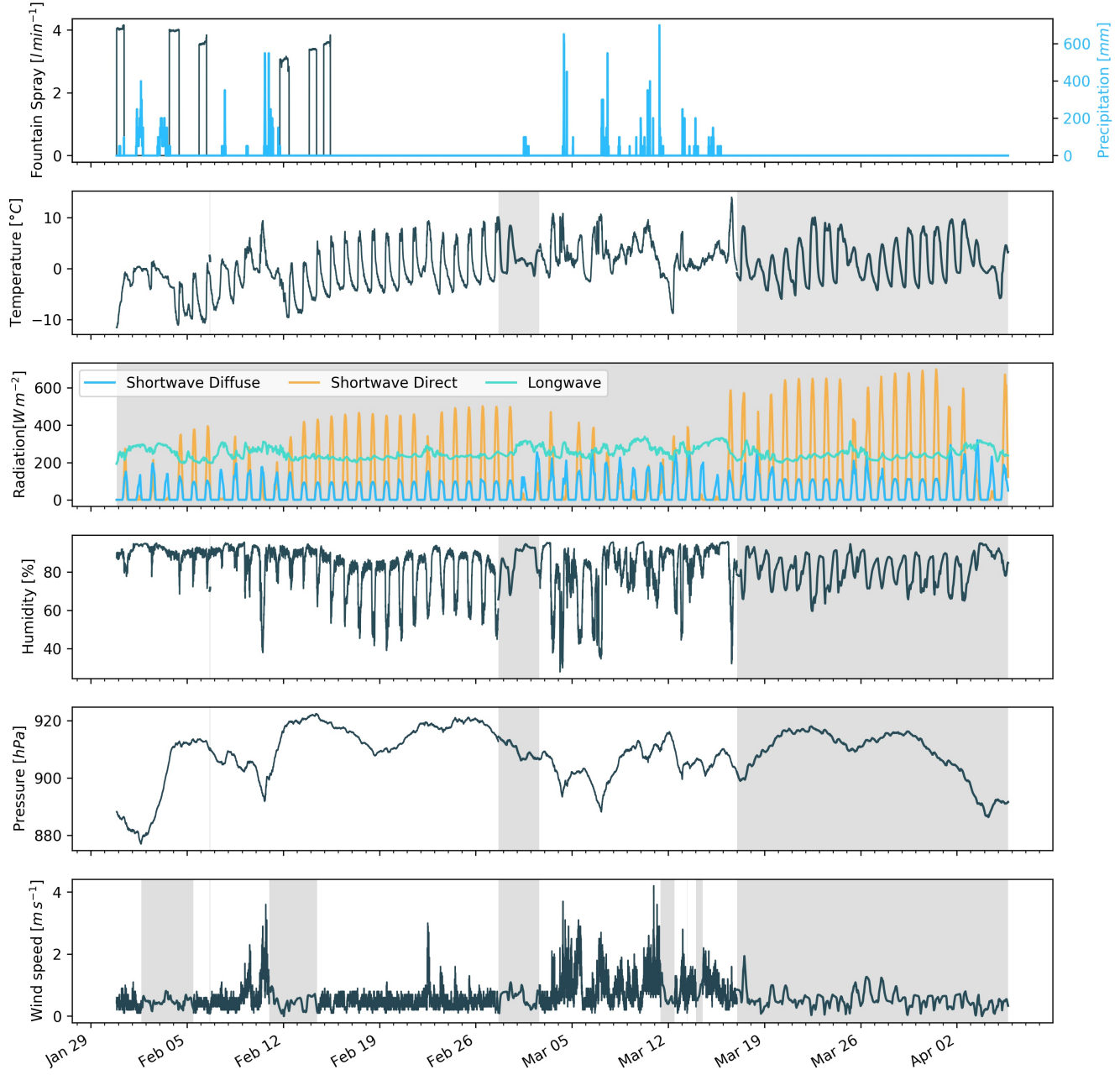


Figure 3. Measurements at the AWS of EP were used as main model input data in 5 minute frequency. Plaffeien AWS provided the precipitation data. Incoming shortwave and longwave radiation were obtained from ERA5 reanalysis dataset. Several data gaps and errors were also filled from the ERA5 dataset (shaded regions).

116 Manual measurements were performed at the end of the freezing period on 14th February 16:00 2019
 117 (only one more fountain run was possible after this date) to estimate r, R, h, H_i, H_f (see Fig. 2 for the
 118 different geometry components):

$$0.55 \leq r \leq 1\text{m} ; 1.1 \leq R \leq 1.2\text{m} ; 0.1 \leq h \leq 0.2\text{m} ; 0.6 \leq H_i \leq 0.8\text{m} ; 1.3 \leq H_f \leq 1.4\text{m}$$

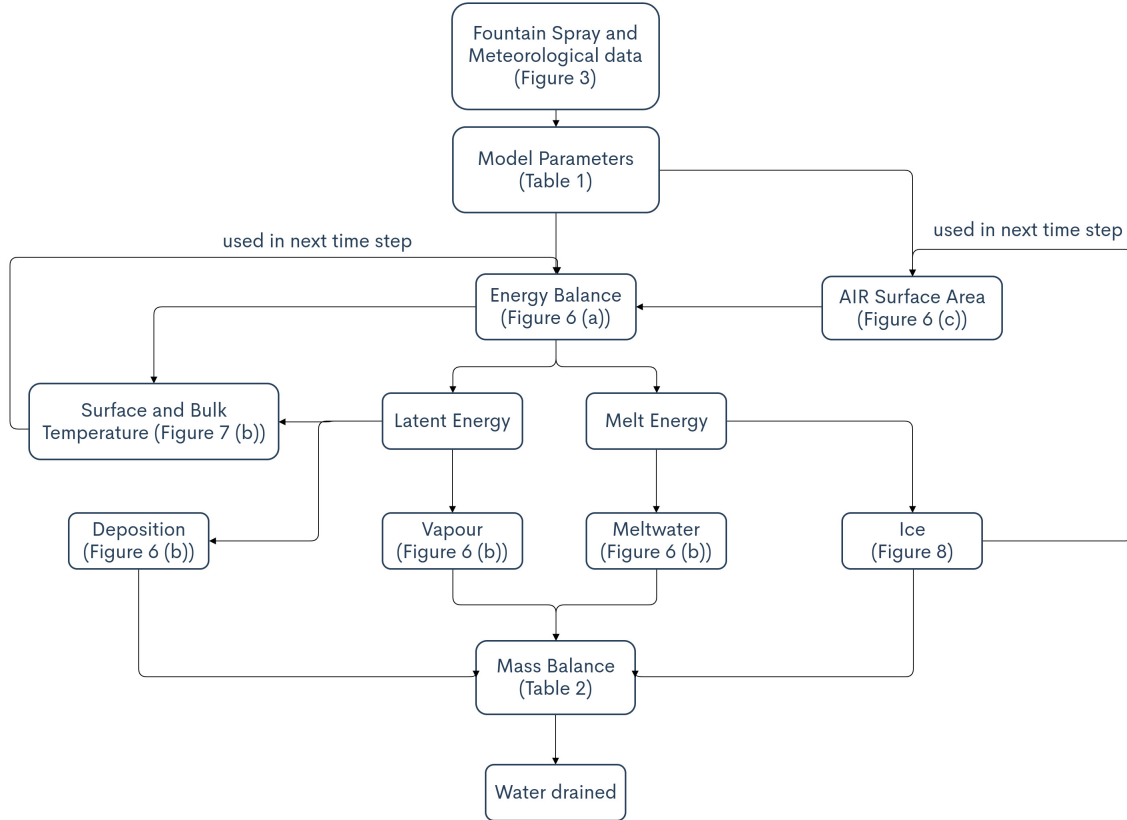


Figure 4. Model schematic showing the algorithm used in the model at every time step. Further details about these variables can be found in the associated tables and figures.

119 The ranges of the variables show its variance across different compass orientations. Correspondingly, the
120 volume range estimated for the first validation point was $0.857 \pm 0.186 m^3$ on 14th February 16:00 2019.

121 The second validation point corresponds to the end of the melting process on 10th March 18:00 2019.
122 Based on the webcam imagery and manual measurement, a thin layer of ice with an observed thickness
123 between 0.01 to 0.06 m could be quantified. This results in the volume range for the second validation to
124 be $0.13 \pm 0.09 m^3$ on 11th March 2019

125 In reality, the EP ice structure was more cylindrical until a height of 0.2 m and conical afterwards until a
126 height of 0.6 m with a radius of 1.18 m. However, we assume a conical shape of this ice structure in order
127 to apply the modelling strategy described below.

3 MODEL SETUP

128 The model (implemented in python) consists of three parts calculating a) the geometric evolution of the
129 Icestupa, b) the energy balance and c) the mass balance as shown schematically in Fig. 4. A bulk energy
130 and mass balance model is used to calculate the amounts of ice, liquid water, water vapour and runoff water
131 of the Icestupa every 5 minutes. The equations used henceforth display model time step superscript only if
132 it is different from the current time step.

133 3.1 Icestupa geometric evolution

134 Radius r_{ice} and height h_{ice} define the dimensions of the Icestupa assuming its geometry to be a cone as
135 shown in Fig. 5. The surface area A exposed to the atmosphere and volume V are:

$$A = \pi \cdot r_{ice} \cdot \sqrt{r_{ice}^2 + h_{ice}^2} \quad (4)$$

$$V = \pi/3 \cdot r_{ice}^2 \cdot h_{ice} \quad (5)$$

136 With the mass of the Icestupa M_{ice} , its current volume can also be expressed as:

$$V = M_{ice}/\rho_{ice} \quad (6)$$

137 where ρ_{ice} is the density of ice (917 kg m^{-3}). The model of the Icestupa is initialised with a thickness
 138 of Δx (defined in 3.2) and a circular area of radius r_F . The constant r_F represents the mean spray radius
 139 of the fountain. This fountain spray radius is determined by modelling the projectile motion of the water
 140 droplets. Using mass conservation the droplet speed v_F can be determined from the spray rate d_F and the
 141 diameter dia_F of the nozzle as follows:

$$v_F = \frac{d_F}{\pi \cdot dia_F^2/4} \quad (7)$$

142 Afterwards, we assume that the water droplets move with an air friction free projectile motion from
 143 the fountain nozzle with a height h_F to the ice/ground surface. The resulting spray radius r_F was then
 144 determined from the projectile motion equation as follows:

$$r_F = \frac{v_F \cdot \cos\theta_F (v_F \cdot \sin\theta_F + \sqrt{(v_F \cdot \sin\theta_F)^2 + 2 \cdot g \cdot h_F})}{g} \quad (8)$$

145 where $g = 9.8 \text{ ms}^{-2}$ is the acceleration due to gravity and $\theta_F = 45^\circ$ is the angle of launch.

146 During subsequent time steps, the dimensions of the Icestupa evolve assuming a uniform ice formation
 147 and decay across its surface area with an invariant slope $s_{cone} = \frac{h_{ice}}{r_{ice}}$ as shown in Fig. 5. During these time
 148 steps, the volume is parameterised using Eqn. 5 as:

$$V = \pi/3 \cdot r_{ice}^3 \cdot s_{cone} \quad (9)$$

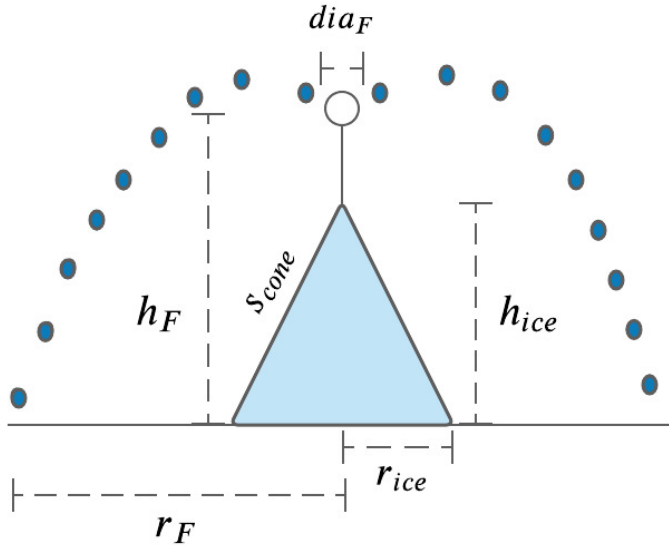


Figure 5. Shape and fountain parameters of the EP Icestupa. r_{ice} is the radius, h_{ice} is the height and s_{cone} is the slope of the ice cone. r_F is the spray radius, h_F is the height and dia_F is the nozzle diameter of the fountain.

149 However, the Icestupa cannot outgrow the maximum range of the water droplets ($(r_{ice})_{max} = r_F$).
 150 Combining equations 5, 6 and 9, the geometric evolution of the Icestupa at each time step i can be
 151 determined by considering the following rules:

$$(r_{ice}, h_{ice}) = \begin{cases} (r_F, \Delta x) & \text{if } i = 0 \\ (r_{ice}^{i-1}, \frac{3 \cdot M_{ice}}{\pi \cdot \rho_{ice} \cdot (r_{ice}^{i-1})^2}) & \text{if } r_{ice}^{i-1} \geq r_F \text{ and } \Delta M_{ice} > 0 \text{ where } \Delta M_{ice} = M_{ice}^{i-1} - M_{ice}^{i-2} \\ (\frac{3 \cdot M_{ice}}{\pi \cdot \rho_{ice} \cdot s_{cone}})^{1/3} \cdot (1, s_{cone}) & \text{otherwise} \end{cases} \quad (10)$$

152 3.2 Energy Balance

153 The energy balance equation for the Icestupa is formulated as follows:

$$q_{net} = q_{SW} + q_{LW} + q_L + q_S + q_F + q_G \quad (11)$$

154 where q_{net} is the net energy flux in $[W m^{-2}]$; q_{SW} is the net shortwave radiation; q_{LW} is the net longwave
 155 radiation; q_L and q_S are the turbulent latent and sensible heat fluxes. q_F represents the heat exchange of the
 156 fountain water droplets with the AIR ice surface during fountain on time steps. q_G represents ground heat
 157 flux between Icestupa surface and Icestupa interior. Energy transferred in the direction of the ice surface is
 158 always denoted as positive and away as negative.

159 Equation 11 is usually referred to as the energy budget for “the surface”, but practically it must apply to a
 160 surface layer of ice with a finite thickness Δx . The energy flux acts upon the Icestupa surface layer which
 161 has an upper and a lower boundary defined by the atmosphere and the ice body of the Icestupa, respectively.
 162 The parameter selection for Δx is based on the following two arguments: (a) the ice thickness Δx should

163 be small enough to represent the daily surface temperature variations and (b) Δx should be large enough
 164 for these temperature variations to not reach the bottom of the surface layer. Therefore, we introduced a 5
 165 mm thick ice surface layer, over which the energy balance is calculated. A sensitivity analysis was later
 166 performed to understand the influence of this factor. Here, we define the surface temperature T_{ice} to be
 167 the modelled average temperature of the Icestupa surface layer and the energy flux q_{net} is assumed to act
 168 uniformly across the Icestupa area A .

169 3.2.1 Net Shortwave Radiation q_{SW}

170 The net shortwave radiation q_{SW} is computed as follows:

$$171 \quad q_{SW} = (1 - \alpha) \cdot (SW_{direct} \cdot f_{cone} + SW_{diffuse}) \quad (12)$$

171 where SW_{direct} and $SW_{diffuse}$ are the ERA5 direct and diffuse short wave radiation, α is the modelled
 172 albedo and f_{cone} is the area fraction of the ice structure exposed to the direct shortwave radiation.

173 We model the albedo using a scheme described in Oerlemans and Knap (1998). The scheme records the
 174 decay of albedo with time after fresh snow is deposited on the surface. δt records the number of time steps
 175 after the last snowfall event. After snowfall, albedo changes over a time step, δt , as

$$\alpha = \alpha_{ice} + (\alpha_{snow} - \alpha_{ice}) \cdot e^{(-\delta t)/\tau} \quad (13)$$

176 where α_{ice} is the bare ice albedo value (0.35), α_{snow} is the snow ice albedo value (0.85) and τ is a decay
 177 rate, which determines how fast the albedo of the ageing snow reaches this value. The decay rate τ is
 178 assumed to have a base value of 10 days similar to values obtained by Schmidt et al. (2017) for wet surfaces
 179 and its maximal value is set based on observations by Oerlemans and Knap (1998) as shown in Table 1.
 180 Furthermore, the albedo α varies depending on the water source that formed the current Icestupa surface.
 181 Correspondingly, the albedo is reset to the value of bare ice albedo if the fountain is spraying water onto
 182 the current ice surface and to the value of fresh snow albedo if a snowfall event occurred. Snowfall events
 183 are assumed if the air temperature is below $T_{rain} = 1^{\circ}C$ (Fujita and Ageta, 2000).

184 The area fraction f_{cone} of the ice structure exposed to the direct shortwave radiation depends on the
 185 shape considered. The direct solar radiation incident on the AIR surface is first decomposed into horizontal
 186 and vertical components using the solar elevation angle θ_{sun} . For a conical shape, half of the total curved
 187 surface is exposed to the vertical component of the direct shortwave radiation and the projected triangle
 188 of the curved surface is exposed to the horizontal component of the direct shortwave radiation. The solar
 189 elevation angle θ_{sun} used is modelled using the parametrisation proposed by Woolf (1968). Accordingly,
 190 f_{cone} is determined as follows:

$$191 \quad f_{cone} = \frac{(0.5 \cdot r_{ice} \cdot h_{ice}) \cdot \cos\theta_{sun} + (\pi \cdot r_{ice}^2 / 2) \cdot \sin\theta_{sun}}{\pi \cdot r_{ice} \cdot (r_{ice}^2 + h_{ice}^2)^{1/2}} \quad (14)$$

191 The measured diffuse shortwave radiation is assumed to impact the conical Icestupa surface uniformly.

192 3.2.2 Net Longwave Radiation q_{LW}

193 The net longwave radiation q_{LW} , for which there were no direct measurements available at EP, is
 194 determined as follows:

$$q_{LW} = LW_{in} - \sigma \cdot \epsilon_{ice} \cdot (T_{ice} + 273.15)^4 \quad (15)$$

195 where T_a represents the measured air temperature, T_{ice} is the modelled surface temperature, both
 196 temperatures are given in $^{\circ}\text{C}$, $\sigma = 5.67 \cdot 10^8 \text{ J m}^{-2} \text{ s}^{-1} \text{ K}^{-4}$ is the Stefan-Boltzmann constant, LW_{in}
 197 denotes the incoming longwave radiation derived from the ERA5 dataset and ϵ_{ice} is the corresponding
 198 emissivity value for the Icestupa surface (see Table 1).

199 3.2.3 Turbulent sensible q_S and latent q_L heat fluxes

200 The turbulent sensible q_S and latent heat q_L fluxes are computed with the following expressions proposed
 201 by Garratt (1992):

$$q_S = c_a \cdot \rho_a \cdot p_a / p_{0,a} \cdot \frac{\kappa^2 \cdot v_a \cdot (T_a - T_{ice})}{(\ln \frac{h_{AWS}}{z_{ice}})^2} \quad (16)$$

$$q_L = 0.623 \cdot L_s \cdot \rho_a / p_{0,a} \cdot \frac{\kappa^2 \cdot v_a (p_{v,a} - p_{v,ice})}{(\ln \frac{h_{AWS}}{z_{ice}})^2} \quad (17)$$

202 where h_{AWS} is the measurement height above the ground surface of the AWS (in m), v_a is the wind
 203 speed in m s^{-1} and M_F denotes fountain water spray mass in kg . c_a is the specific heat of air at
 204 constant pressure ($1010 \text{ J kg}^{-1} \text{ K}^{-1}$), ρ_a is the air density at standard sea level (1.29 kg m^{-3}), $p_{0,a}$ is the air
 205 pressure at standard sea level (1013 hPa), κ is the von Karman constant (0.4), L_s is the heat of sublimation
 206 (2848 kJ kg^{-1}) and z_{ice} (1.7 mm) denotes the roughness length of ice (momentum and scalar) described
 207 in (Garratt, 1992). The vapor pressures over air ($p_{v,a}$) and ice ($p_{v,ice}$) was obtained using the following
 208 formulation given in WMO (2018):

$$\begin{aligned} p_{v,a} &= 6.107 \cdot 10^{(7.5 \cdot T_a / (T_a + 237.3))} \\ p_{v,ice} &= (1.0016 + 3.15 \cdot 10^{-6} \cdot p_a - 0.074 \cdot p_a^{-1}) \cdot (6.112 \cdot e^{(22.46 \cdot T_{ice} / (T_{ice} + 272.62))}) \end{aligned} \quad (18)$$

209 where p_a is the measured air pressure in hPa .

210 3.2.4 Fountain water heat flux q_F

211 The total energy flux is further influenced through the heat flux caused by the water that was additionally
 212 added to the surface of the Icestupa during the time the fountain was running. We take this interaction
 213 between the fountain water and the ice surface into account by assuming that the ice surface temperature
 214 stays constantly at 0°C during time steps when the fountain is active. This process can be divided into two
 215 simultaneous steps: (a) the water temperature T_{water} is cooled to 0°C and (b) the ice surface temperature is
 216 warmed to 0°C . Process (a) transfers hereby the necessary energy for process (b) throughout the fountain
 217 runtime. We further assume that this process is instantaneous, i.e. the ice temperature is immediately set
 218 to 0°C within just one time step Δt when the fountain is switched on. Thus, the heat flux caused by the
 219 fountain water is calculated as follows:

$$q_F = \begin{cases} 0 & \text{if } \Delta M_F = 0 \\ \frac{\Delta M_F \cdot c_{water} \cdot T_{water}}{\Delta t \cdot A} + \frac{\rho_{ice} \cdot \Delta x \cdot c_{ice} \cdot T_{ice}}{\Delta t} & \text{if } \Delta M_F > 0 \end{cases} \quad (19)$$

220 with c_{ice} as the specific heat of ice.

221 3.2.5 Bulk Icestupa heat flux q_G

222 The bulk Icestupa heat flux q_G corresponds to the ground heat flux in normal soils and is caused by
223 the temperature gradient between the surface layer and the ice body. It is expressed by using the heat
224 conduction equation as follows:

$$225 \quad q_G = k_{ice} \cdot (T_{bulk} - T_{ice}) / l_{ice} \quad (20)$$

226 where k_{ice} is the thermal conductivity of ice in $[W m^{-1} K^{-1}]$, T_{bulk} is the mean temperature of the ice
227 body within the Icestupa and l_{ice} is the average distance of any point in the surface to any other point in the
ice body. T_{bulk} is initialised as $0^\circ C$ and later determined from Eqn. 20 as follows:

$$228 \quad T_{bulk} = T_{bulk}^{i-1} - (q_G \cdot A \cdot \Delta t) / (M_{ice} \cdot c_{ice}) \quad (21)$$

229 Since we assume a conical shape with $r_{ice} > h_{ice}$, l_{ice} cannot be greater than $2r_{ice}$ and also cannot
230 be less than Δx . Therefore, the average distance from any point on the surface to any point inside is
 $231 \Delta x \leq l_{ice} \leq r_{ice}$. We calculate q_G here assuming $l_{ice} = r_{ice}/2$.

232 3.2.6 Surface temperature changes and melt energy q_{melt}

233 The available net energy q_{net} partly increases surface temperature, but also contributes to ice melt at the
234 surface of the Icestupa. q_T denotes the energy used on changing the surface temperature T_{ice} and q_{melt}
denotes the energy used to produce meltwater. So Eqn. 11 can be rewritten as:

$$235 \quad q_{net} = q_{melt} + q_T \quad (22)$$

236 We define the freezing energy as $q_{freeze} = (q_{net} - q_L)$. This is because the latent heat always contributes
237 to temperature fluctuations. Now, the temperature fluctuates based on 3 scenarios namely, (1) the freezing
238 energy flux is negative but cannot freeze all the fountain water output; (2) the freezing energy flux is
239 negative and can freeze all the fountain water output; (3) the freezing energy is positive and (4) the fountain
is inactive ($\Delta M_F = 0$). Therefore, we express the rate of change of temperature as follows:

$$\frac{\Delta T}{\Delta t} = \begin{cases} -T_{ice}^{i-1} / \Delta t & \text{if } q_{freeze} < 0 \text{ and } \Delta M_F \geq -q_{freeze} \cdot A \cdot \Delta t / L_f \\ (\Delta M_F \cdot L_f) / (\rho_{ice} \cdot c_{ice} \cdot \Delta x \cdot A \cdot \Delta t) & \text{if } q_{freeze} < 0 \text{ and } \Delta M_F < -q_{freeze} \cdot A \cdot \Delta t / L_f \\ q_{net} / (\rho_{ice} \cdot c_{ice} \cdot \Delta x) & \text{if } \Delta M_F = 0 \text{ or } q_{freeze} > 0 \end{cases} \quad (23)$$

240 Whenever the model predicts $T_{ice}^{i+1} > 0^\circ C$, then the surface temperature is set to $0^\circ C$ in the corresponding
241 time step and additional energy contributes to q_{melt} . Combining these requirements, we get:

$$(q_T, q_{melt}) = \begin{cases} (\rho_{ice} \cdot c_{ice} \cdot \Delta x \cdot \frac{\Delta T}{\Delta t}, q_{net} - q_L - \rho_{ice} \cdot c_{ice} \cdot \Delta x \cdot \frac{\Delta T}{\Delta t}) & \text{if } T_{ice}^{i+1} \leq 0^\circ C \text{ and } \Delta M_F > 0 \\ (\rho_{ice} \cdot c_{ice} \cdot \Delta x \cdot \frac{\Delta T}{\Delta t}, q_{net} - \rho_{ice} \cdot c_{ice} \cdot \Delta x \cdot \frac{\Delta T}{\Delta t}) & \text{if } T_{ice}^{i+1} \leq 0^\circ C \text{ and } \Delta M_F = 0 \\ (-\rho_{ice} \cdot c_{ice} \cdot \Delta x \cdot \frac{T_{ice}^i}{\Delta t}, q_{net} - q_L + \rho_{ice} \cdot c_{ice} \cdot \Delta x \cdot \frac{T_{ice}^i}{\Delta t}) & \text{if } T_{ice}^{i+1} > 0^\circ C \text{ and } \Delta M_F > 0 \\ (-\rho_{ice} \cdot c_{ice} \cdot \Delta x \cdot \frac{T_{ice}^i}{\Delta t}, q_{net} + \rho_{ice} \cdot c_{ice} \cdot \Delta x \cdot \frac{T_{ice}^i}{\Delta t}) & \text{if } T_{ice}^{i+1} > 0^\circ C \text{ and } \Delta M_F = 0 \end{cases} \quad (24)$$

Table 1. Free parameters in the model categorised as constant, uncertain and site parameters. Base value (B) and uncertainty (U) were taken from the literature. For assumptions (assum.), the uncertainty was chosen to be relatively large (5 %). For measurements (meas.), the uncertainty due to parallax errors is chosen to be (1 %).

Constant Parameters	Symbol	Value	References
Van Karman constant	κ	0.4	B: Cuffey and Paterson
Stefan Boltzmann constant	σ	$5.67 \cdot 10^{-8} W m^{-2} K^{-4}$	B: Cuffey and Paterson
Air pressure at sea level	$p_{0,a}$	1013 hPa	B: Mölg and Hardy
Density of water	ρ_w	$1000 kg m^{-3}$	B: Cuffey and Paterson
Density of ice	ρ_{ice}	$917 kg m^{-3}$	B: Cuffey and Paterson
Density of air	ρ_a	$1.29 kg m^{-3}$	B: Mölg and Hardy
Specific heat of water	c_w	$4186 J kg^{-1} ^\circ C^{-1}$	B: Cuffey and Paterson
Specific heat of ice	c_{ice}	$2097 J kg^{-1} ^\circ C^{-1}$	B: Cuffey and Paterson
Specific heat of air	c_a	$1010 J kg^{-1} ^\circ C^{-1}$	B: Mölg and Hardy
Thermal conductivity of ice	k_{ice}	$2.123 W m^{-1} K^{-1}$	B: Bonales et al.
Latent Heat of Sublimation	L_s	$2848 kJ kg^{-1}$	B: Cuffey and Paterson
Latent Heat of Evaporation	L_e	$2514 kJ kg^{-1}$	B: Cuffey and Paterson
Latent Heat of Fusion	L_f	$334 kJ kg^{-1}$	B: Cuffey and Paterson
Gravitational acceleration	g	$9.81 m s^{-2}$	B: Cuffey and Paterson
Uncertain Parameters			Range
Precipitation	T_{rain}	$1 ^\circ C$	$\pm 1 ^\circ C$
Temperature threshold			B + U: Fujita and Ageta, Zhou et al.
Ice Emissivity	ϵ_{ice}	0.95	$\pm 5 \%$
Ice Albedo	α_{ice}	0.35	$\pm 5 \%$
Snow Albedo	α_{snow}	0.85	$\pm 5 \%$
Albedo Decay Rate	τ	10 days	[1, 22] days
Ice layer thickness	Δx	5 mm	[1, 10] mm
Site Parameters			
Fountain diameter	nozzle	dia_F	5 mm
Fountain height		h_F	$\pm 1 \%$
Fountain temperature	water	T_{water}	$1.35 m$
AWS height		h_{AWS}	$5 ^\circ C$
			[0, 9] °C
			$\pm 1 \%$
			B: meas. ; U: assum.
			B: meas. ; U: assum.
			B: meas. ; U: meas.
			B: meas. ; U: assum.

242 3.3 Mass Balance

243 The mass balance equation is used to derive the water that drains away M_{runoff} as follows:

$$\frac{\Delta M_{runoff}}{\Delta t} = \frac{\Delta M_F + \Delta M_{ppt} + \Delta M_{dpt} - \Delta M_{ice} - \Delta M_{melt} - \Delta M_{vapour}}{\Delta t} \quad (25)$$

244 where $\Delta M = M^i - M^{i-1}$. Here $\frac{\Delta M_F}{\Delta t} = d_F$ where d_F is the spray of the fountain measured in $[kg s^{-1}]$; 245 M_{ppt} is the cumulative precipitation and M_{dpt} is the cumulative accumulation through water vapour 246 condensation or deposition; M_{ice} is the cumulative mass of ice; M_{melt} is the cumulative mass of melt water 247 and M_{vapour} represents the cumulative water vapor loss by evaporation or sublimation.

248 Precipitation input is calculated as:

$$\frac{\Delta M_{ppt}}{\Delta t} = \begin{cases} \pi \cdot r_{ice}^2 \cdot \rho_w \cdot ppt & \text{if } T_a < T_{rain} \\ 0 & \text{if } T_a \geq T_{rain} \end{cases} \quad (26)$$

249 where ρ_w is the density of water ($1000 kg m^{-3}$), ppt is the measured precipitation rate in $[m s^{-1}]$ and 250 T_{rain} is the temperature threshold below which precipitation falls as snow. Here, snowfall events were 251 identified using T_{rain} as $1^\circ C$. Snow mass input is calculated by assuming a uniform deposition over the 252 entire circular footprint of the Icestupa.

253 The latent heat flux is used to estimate either the evaporation and condensation processes or sublimation 254 and deposition processes. To differentiate between these two possibilities, we classify the time steps 255 into humid or non-humid if the condensation or evaporation to occur whereas on non-humid time steps 256 deposition or sublimation can occur. Correspondingly, latent heat of evaporation (L_e) is used for humid 257 time steps and latent heat of sublimation (L_s) is used for non-humid time steps. Water accumulation and 258 vapour loss from the Icestupa surface is calculated as follows:

$$\left(\frac{\Delta M_{vapour}}{\Delta t}, \frac{\Delta M_{dpt}}{\Delta t} \right) = \begin{cases} (-q_L \cdot A/L, 0) & \text{if } q_L < 0 \\ (0, q_L \cdot A/L) & \text{if } q_L \geq 0 \end{cases} \quad (27)$$

259 where $L = \begin{cases} L_s & \text{if } RH < 60 \\ L_e & \text{if } RH \geq 60 \end{cases}$

260 Using the melt energy q_{melt} , we estimate the frozen and melted ice mass (ΔM_{ice} , ΔM_{melt}). Removing 261 the contribution of precipitation and combining Eqn. 27 we are left with the contribution from the melt 262 energy as follows:

$$\left(\frac{\Delta M_{ice} - \Delta M_{ppt} - \Delta M_{dpt} + \Delta M_{vapour}}{\Delta t}, \frac{\Delta M_{melt}}{\Delta t} \right) = \begin{cases} \frac{q_{melt} \cdot A}{L_f} \cdot (-1, 1) & \text{if } q_{melt} \geq 0 \\ \frac{q_{melt} \cdot A}{L_f} \cdot (-1, 0) & \text{if } q_{melt} < 0 \text{ and } \frac{\Delta M_F}{\Delta t} \geq -\frac{q_{melt} \cdot A}{L_f} \\ \left(\frac{\Delta M_F}{\Delta t}, 0 \right) & \text{if } q_{melt} < 0 \text{ and } 0 \leq \frac{\Delta M_F}{\Delta t} < -\frac{q_{melt} \cdot A}{L_f} \\ \frac{\Delta M_{melt} + \Delta M_{vapour}}{\Delta t} & \text{if } RH \geq 60 \end{cases} \quad (28)$$

Table 2. Summary of calculated mass balance components for the EP experiment after the fountain spray was stopped on 15th February 2019 and at the end of the model run on 5th April.

	Mass Component	Fountain spray ends	Model ends
Input	M_F	18060 kg	18060 kg
	M_{ppt}	444 kg	467 kg
	M_{dpt}	7 kg	33 kg
Output	M_{melt}	165 kg	1023 kg
	M_{ice}	814 kg	0 kg
	M_{vapour} M_{runoff}	3 kg 17529 kg	8 kg 17529 kg

263 Now, with all the other terms known in Eqn. 25, the water drainage/runoff can now be determined.
 264 Considering AIRs as water reservoirs, we can quantify their potential through the amount of water they
 265 store (storage quantity) and the length of time they store it (storage duration). Another means of comparing
 266 different Icestupas is through their water storage efficiency defined accordingly as:

$$\text{Storage Efficiency} = \frac{M_{melt}}{(M_F + M_{ppt} + M_{dpt})} \cdot 100 \quad (29)$$

4 MODEL RESULTS

267 The model was forced with meteorological data from 30th January to 5th April 2019 (Fig. 3) and various
 268 parameters (see Table 1) to calculate the mass and energy balance of the Icestupa.

4.1 Energy and mass balance calculation

269 Daily averages of some components of the energy balance are shown in Fig. 6 (a). On average during the
 270 experiment duration, the total energy flux between the atmosphere and the Icestupa are almost balanced.
 271 Net shortwave radiation (28 W m^{-2}), sensible (17 W m^{-2}) and latent heat flux (9 W m^{-2}) with a mostly
 272 positive flux towards the surface of the icerustupa are compensated by the net longwave radiation (- 36
 273 W m^{-2}) and the melt energy (- 19 W m^{-2}). The contribution of other fluxes are negligible in comparison.
 274

275 Net shortwave radiation is the main input to, and the most varying energy flux on the ice surface. Its
 276 variability is controlled by the surface albedo α and the area fraction f_{cone} which therefore represent key
 277 variables in the energy balance (Fig. 7 (a)). Although global radiation flux reached a daily maximum
 278 value of 304 W m^{-2} , q_{SW} only went up to 68 W m^{-2} . This is caused by the fact that only about 30 % of
 279 the direct solar radiation influenced the Icestupa surface as shown by the area fraction f_{cone} in Fig. 7 (a).
 280 Snowfall is the atmospheric variable connected most closely and proportionally to albedo. Higher and/or
 281 more frequent snowfall thus decreases the energy available for melt due to the corresponding increase in α .

282 q_{LW} was predominantly negative indicating that this energy balance component drove the freezing of the
 283 ice structure. The incoming longwave radiation was strongly dependent on atmospheric emissivity which
 284 had a mean value of 0.77. Atmospheric emissivity in turn depended on the cloudiness factor. Daily values
 285 of q_{LW} ranged from -95 to 7 W m^{-2} . q_{LW} and q_S were both proportional to the temperature gradient
 286 between the air and the Icestupa surface. Turbulent sensible heat flux q_S contributed mostly to the melt
 287 of the ice structure. Daily values of q_S ranged from -16 to 59 W m^{-2} . Turbulent latent heat flux q_L was

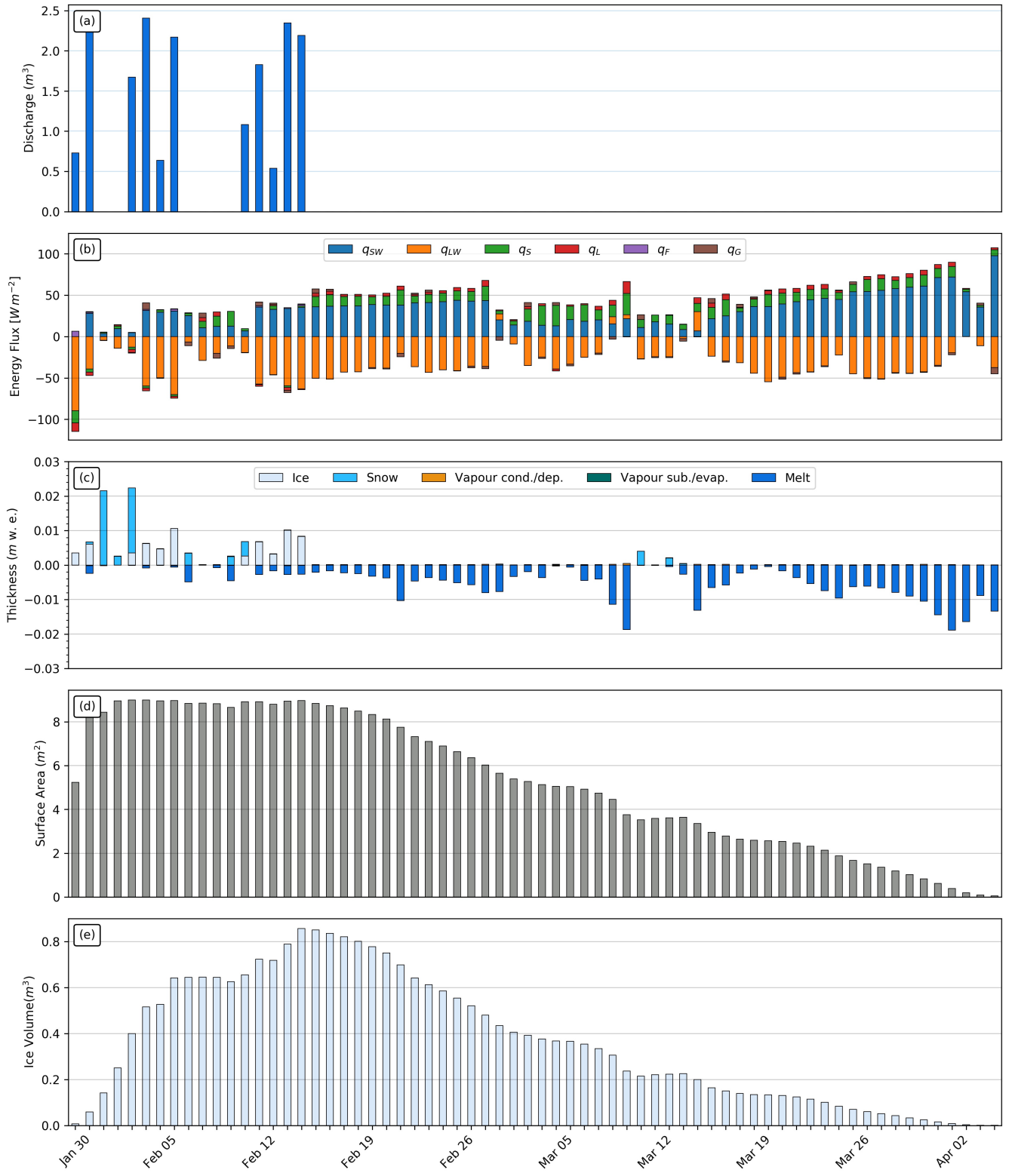


Figure 6. (a) Fountain discharge (b) energy flux components, (c) mass flux components (d) surface area and (e) volume of the Icestupa in daily time steps. q_{SW} is the net shortwave radiation; q_{LW} is the net longwave radiation; q_L and q_S are the turbulent latent and sensible heat fluxes. q_F represents the interactions of the ice-water boundary during fountain on time steps. q_G quantifies the heat conduction process between the Icestupa surface layer and the ice body.

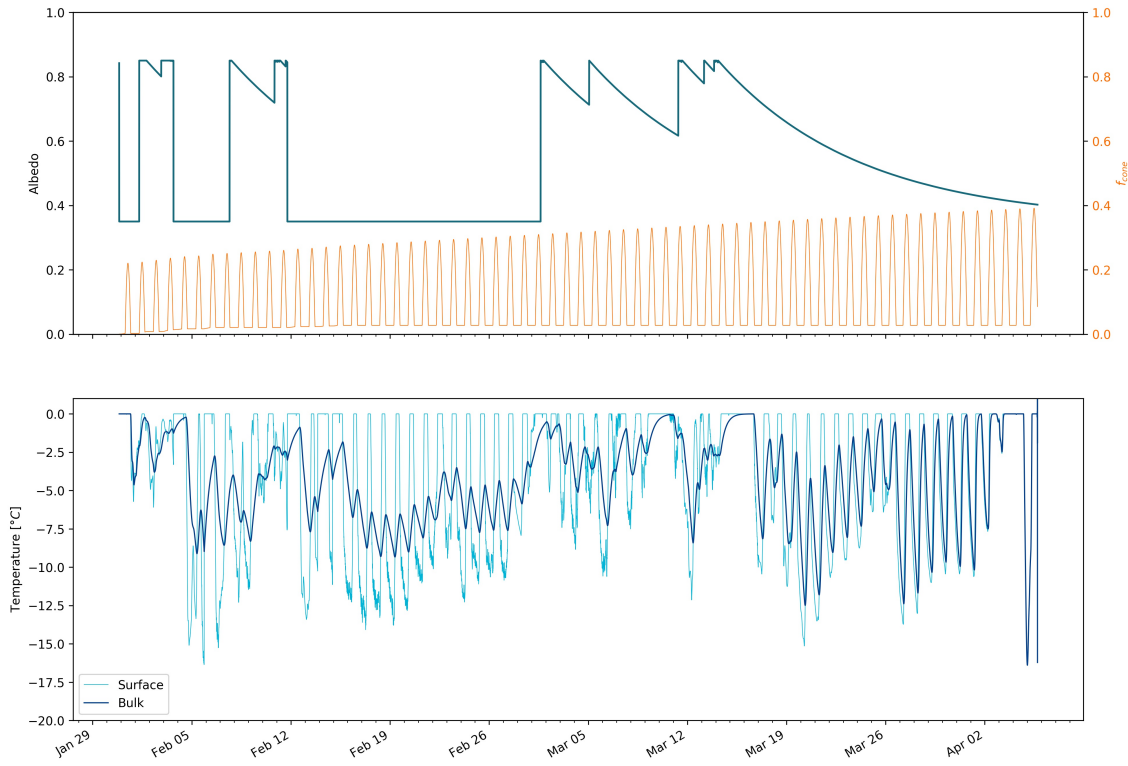


Figure 7. Some derived parameters of the model, namely, albedo and f_{cone} (a), Surface and bulk temperature (b). In (a), the black curve shows how snow and fountain-on events reset albedo between ice albedo and snow albedo. The decay of the snow albedo to ice albedo can also be observed. The blue curve shows how the solar radiation area fraction varied diurnally with variations in the solar elevation angle. In (b), the surface temperature (black curve) was forced to be 0 °C during fountain activity. The corresponding bulk temperature is shown with the blue curve.

288 predominantly positive suggesting that it favoured deposition/condensation over evaporation/sublimation.
 289 Daily values of q_L ranged from -4 to 47 $W m^{-2}$. Therefore, the Icestupa gained mass cumulatively from
 290 the atmosphere due to the deposition/condensation process. Fountain water heat flux q_F had a mean of
 291 zero as it was only nonzero during 1002 time steps or around 100 hours. Daily values of q_F ranged from
 292 0 to 7 $W m^{-2}$. The contribution of heat flux by conduction q_G was minimal as it only varied between
 293 -7 to 7 $W m^{-2}$ with a mean of 0 $W m^{-2}$. The energy contributing to surface temperature changes (q_T)
 294 was insignificant in comparison to the energy spent on freezing and melting (q_{melt}). The resulting bulk
 295 temperature and the surface temperature are shown in Fig. 7 (b). For the total considered period, q_{LW}
 296 accounted for 28.3% of overall energy turnover. The energy turnover is calculated as the sum of energy
 297 fluxes in absolute values. q_{SW} accounted for 21.7%, followed by q_{melt} (25.4%), q_S (14.6%), q_L (7.5%), q_G
 298 (1.8%), q_F (0.3%) and q_T (0.3%).

299 Fig. 6 (b) represents the mass fluxes associated with these energy exchanges expressed in m w.e. It
 300 shows the ice and meltwater formed due to q_{melt} , snow accumulated due to precipitation, water vapour
 301 deposition/condensation and sublimation/evaporation due to q_L . Growth rate ($\frac{\Delta M_{ice}}{\Delta t}$) shows a strong
 302 correlation with net energy flux ($r^2 = 0.44$) but poor correlation with Icestupa surface area ($r^2 = 0.04$).
 303 This is because the variance in growth rate is mostly due to the variance in q_{net} as illustrated in Fig. 6.
 304 Since r_{ice} was initialised with the spray radius r_F , the surface area maintains a maximum initially until the

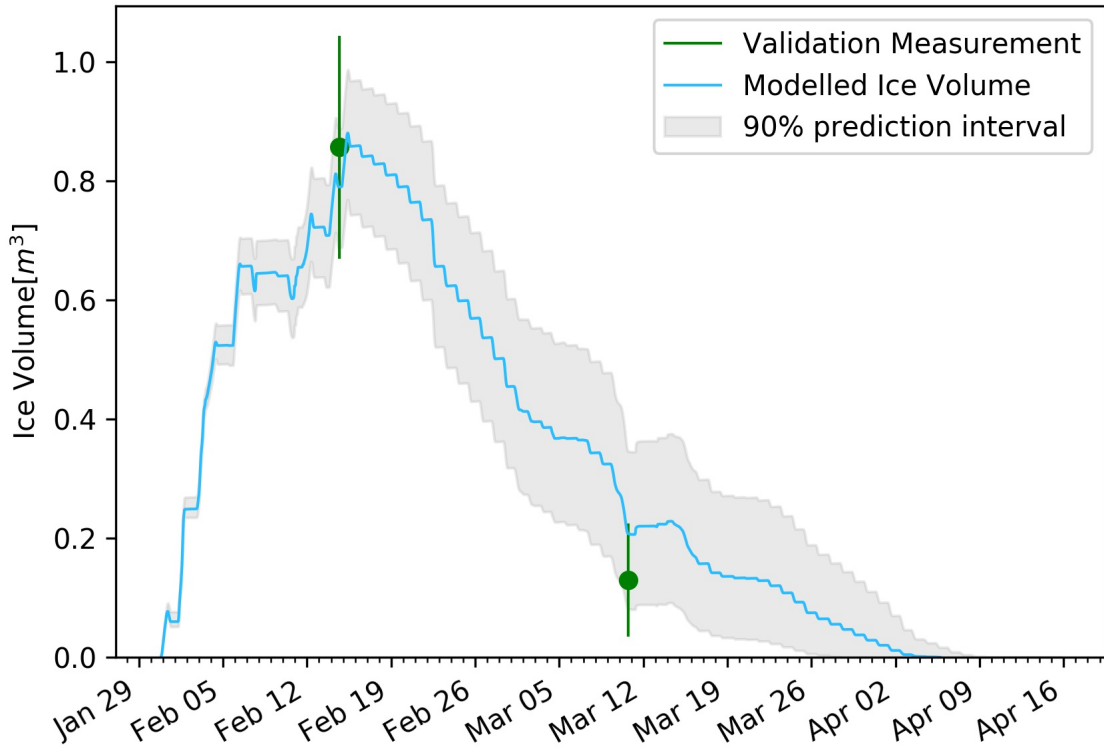


Figure 8. Modelled ice volume during the lifetime of the EP Icestupa (blue curve). Green line segments indicate the first and second validation measurements. The prediction interval is based on the ice volume uncertainty caused by the most sensitive parameters, namely, temperature threshold below which precipitation falls as snow and the ice emissivity.

305 energy flux becomes positive. This trend favours the positive over the negative thickness changes resulting
306 in a steep increase and gradual melting of ice volume as can be seen in Fig. 8.

307 The total water used for the Icestupa development includes contributions from the fountain (97.2%),
308 snowfall (2.5 %) and deposition/condensation (0.3 %) as shown in Table 2. The maximum ice mass during
309 the whole measurement period was 1158 kg, which occurred after the last fountain run on Feb 16th in
310 the morning. Therefore, in the case of EP we used a water input of 18,584 kg, with a resultant storage
311 efficiency of only 7.5 %.

5 MODEL SENSITIVITY AND UNCERTAINTY ANALYSIS

312 The icestupa model can be regarded as a function $f(x_1, x_2 \dots, x_n) = (y_1, y_2 \dots, y_m)$, where
313 $(x_1, x_2 \dots, x_n)$ are the model parameters and $(y_1, y_2 \dots, y_m)$ are the model outputs. The influence of each
314 parameter on the output variables of interest were quantified and the most important physical parameters
315 for the subsequent uncertainty analysis were determined. The sensitivity of a parameter x_j is determined
316 by keeping all other parameters $x_i, i \neq j$ fixed at their baseline value and varying x_j within values that are
317 physically plausible.

318 A sensitivity study on the parameters (listed in Table 1) was performed with the maximum ice volume
319 as the target variable. All the parameters were assumed to be independent of each other with a uniform
320 distribution. This assumption ignores the auto-correlation present among the parameters associated with
321 the albedo parameterisation. The range of uncertain parameters were set based on available literature values

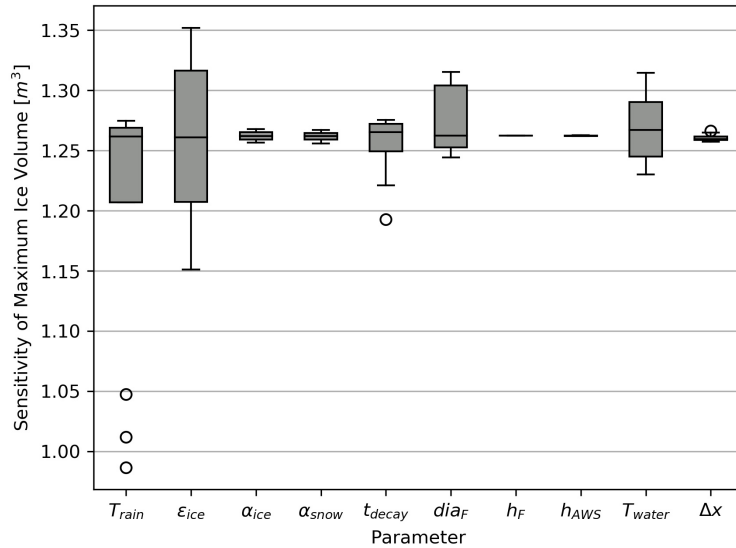


Figure 9. Sensitivities of maximum ice volume to all the uncertain and site parameters used in the model (Table 1). Outliers in the bar plot are shown as 'o'.

322 or varied $\pm 5\%$ from the base value if no such reference was available. The uncertainty of all the site
 323 parameters were caused due to parallax errors during manual measurement. This was quantified with a
 324 range of $\pm 1\%$ from the base value. However, it must be kept in mind that, even though intended to be as
 325 objective as possible, the selection of a parameter range has a subjective part that influences the results and
 326 conclusions obtained in this analysis. The variation of the model outputs y_k is evaluated to quantify the
 327 local sensitivities $s_{j,k}$ that are defined here as the 95% range of the simulated outputs.

328 To perform the uncertainty analysis, we included only parameters that influence the maximum ice volume
 329 by at least $0.1 m^3$. All other parameters were fixed at their baseline value. Fig. 9 shows all the variance
 330 produced by these uncertain parameters in maximum ice volume calculation. It shows that ϵ_{ice} and T_{train}
 331 are the only parameters with a maximal sensitivity of more than $0.1 m^3$ for the maximum ice volume
 332 estimate. Consequently, all other parameters were excluded from the subsequent uncertainty analysis.

333 The temperature threshold below which precipitation falls as snow (T_{train}) was found to be the most
 334 sensitive parameter. It is used in the model to reset the albedo to snow albedo and determine snow
 335 precipitation events. The lower T_{train} parameter the higher the albedo (as the Icestupa surface has a lower
 336 albedo when ice-covered than when snow-covered) . The variation of T_{train} by $\pm 1^\circ C$ caused maximum
 337 ice volume variation of $1.2 \pm 0.2 m^3$.

338 Ice emissivity was also found to be a sensitive parameter. The higher the ice emissivity the larger the
 339 maximum ice volume as the emitted longwave radiation increases with ice emissivity. Variation of ϵ_{ice} by
 340 5% caused a maximum ice volume range from $1.3 \pm 0.1 m^3$.

341 In total, the sensitivity analysis required 120 simulations, and the uncertainty analysis a total of 32
 342 simulations.

6 DISCUSSION

343 6.1 Model validation quality

344 We first evaluate the model against the validation measurements at the EP site. The uncalibrated model is
 345 able to capture both the freezing and the melting process sufficiently well as the modelled ice volume lies
 346 within the uncertainty of both validation measurements. Furthermore, the validation measurements fit well
 347 within the estimated model uncertainty. However, since this validation is based on only two points, it does
 348 limit the confidence in the model results. Moreover, the model seems to overestimate the ice volume at
 349 both validation points. This could be due to the underestimation of the surface area which underestimates
 350 the melt rates (absolute growth rate when $\frac{\Delta M_F}{\Delta t} < 0$) and the freeze rates (absolute growth rate when
 351 $\frac{\Delta M_F}{\Delta t} > 0$). However, as the fountain was mostly inactive during the study period, the underestimation
 352 of surface area disproportionately undervalues the melt rates over the freeze rates. One major cause of
 353 this underestimation was the conical shape assumption, as in reality, the Icestupa shape ranged between a
 354 cone and a cylinder (Fig. 2). Another cause was the surface irregularities that were observed due to uneven
 355 exposure to direct solar radiation and fountain droplets. The sensitivity of the model results to these errors
 356 was further amplified due to the relatively small volume of the EP Icestupa. In summary, more validation
 357 measurements on a more voluminous Icestupa would have increased confidence on the model results.

358 6.2 Important assumptions

359 In the sensitivity and uncertainty analysis presented above, we did not account for several general
 360 assumptions and parametrisation choices that may cause model errors. Some assumptions and their
 361 potential to cause errors are discussed below.

- 362 • Turbulent Sensible and Latent Heat Fluxes: The method used to calculate the turbulent heat fluxes
 363 by Garratt (1992) assumes that the turbulent heat fluxes are acting over a uniform planar surface to
 364 determine the roughness length. Since our application is on a conical surface, the distance to the ice
 365 surface is not uniform and well defined. Hence, z_{ice} has no real physical significance here.
- 366 • Droplet flight time loss: Water losses during the flight time of fountain droplets were neglected making
 367 all the fountain spray available for freezing. For the EP experiment, inclusion of this parameter does
 368 not influence results since it is already accounted for in the runoff water discharge rate which was at
 369 least 3 l min^{-1} .
- 370 • Nucleation of droplets: Corresponding to droplet flight time, ice/snow formation is also possible before
 371 surface contact if nucleation occurs during flight time. For the EP experiment, this process will further
 372 increase the freeze rate and hence the storage efficiency. This process is neglected for model simplicity.

373 6.3 Schwarzsee vs Leh Icestupa

374 It could be argued that the relatively small EP Icestupa cannot be compared with the much larger Icestupas
 375 in Ladakh which store millions of litres of water for several months (see Appendix 8.1). However, this is
 376 the only Icestupa dataset available for such a model validation.

377 Table 2 clearly shows that for our EP experiment most of the input water (92 %) simply runoff away.
 378 This high water loss through drainage is due to the fact that the average spray rate of the fountain
 379 ($(\frac{\Delta M_F}{\Delta t})_{mean} = 3.6 \text{ l min}^{-1}$) far exceeded the max Icestupa growth rate ($(\frac{\Delta M_{ice}}{\Delta t})_{max} = 1 \text{ l min}^{-1}$ (w.e.)).

380 In the city of Leh, Ladakh at an altitude of 3500 m a.s.l. the air temperature shows values down to 27.9
 381 °C in winter (Chevuturi et al., 2018) whereas EP had a minimum temperature of just -11.6 °C during the
 382 study period. Moreover, subzero temperatures were only reached for 7 nights of fountain operation at the
 383 EP site compared to the 43 nights of fountain operation possible in Ladakh (see Appendix 8.1). Thus,

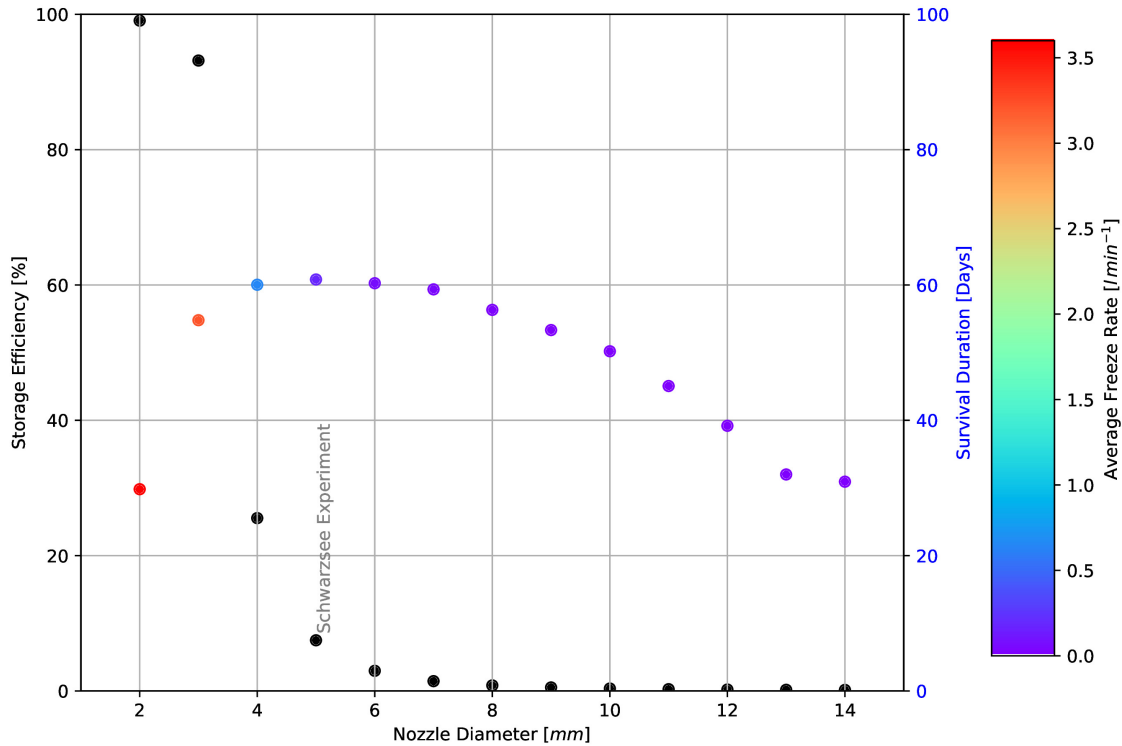


Figure 10. Variation in storage efficiency (black dots) and storage duration (coloured dots) with changes in fountain nozzle's nozzle diameter. The dot colours represent average freeze rate based on the color bar.

384 the Icestupa growth rate is expected to be much higher in Ladakh. However, water spray rates in Ladakh
 385 are also much higher (around 210 l min^{-1}). So the water losses in Ladakh could also be caused due to
 386 excessive fountain spray.

387 **6.4 Icestupa construction decisions**

388 There are several decisions one has to take when constructing Icestupas. These can be broadly divided
 389 into two types of decisions, namely fountain and location decisions. Both the meteorological conditions
 390 of the location and the surface area produced by the fountain significantly influence the observed growth
 391 rate. Since our validation is restricted to just one location, we restrict our discussion to the optimization
 392 possibilities of Icestupa constructions through fountain decisions.

393 Assuming a constant spray for the fountain, we can divide the fountain decisions into fountain state
 394 (on/off) and type (height and nozzle diameter). From an energy balance point of view, the fountain should
 395 be switched on for all time intervals when $q_{net} < 0$. However, in our experiment, the fountain state decision
 396 was set based on whether the ambient temperature was above or below a critical temperature of -5°C .
 397 Ambient temperature can serve as an indicator of q_{net} as it was correlated ($r^2 = 0.53$). However, q_{net}
 398 was found to be negative already at a critical temperature of -1°C . Therefore, using air temperature to
 399 determine when the fountain should be switched on is justified but a higher critical temperature could have
 400 been used in the case of the EP Icestupa.

401 The fountain type used can be characterised by the physical structure of the fountain, namely its height and
 402 nozzle diameter. Maintaining the same spray rate and height, one can optimize the Icestupa development
 403 by identifying the minimum nozzle diameter that yields the maximum storage efficiency.

404 Fig. 10 shows reducing the nozzle diameter to 3 mm increases storage efficiency up to 93 % without
405 compromising much on storage duration. The corresponding storage quantity of the 3 mm nozzle diameter
406 was more than 20 times higher than the 5 mm fountain used in our experiment. This is because the spray
407 radius r_F of the 3 mm fountain was much higher at 8.5 m compared to the 1.7 m spray radius of the
408 5 mm fountain (see Appendix Section ??). Here, we define growth rate as freeze rate when fountain is
409 active and melt rate otherwise. So this higher spray radius both, increases the freeze rate and increases
410 the melt rate since they are both directly proportional to the surface area. However, since the freeze rate
411 cannot increase beyond a spray rate of 3.6 l min^{-1} (except during precipitation or deposition/condensation
412 events), an optimum spray radius or nozzle diameter exists, beyond which storage duration suffers due to a
413 disproportionate increase in melt rate compared to the freeze rate. So even though 3 mm nozzle diameter
414 had a much higher storage quantity than the 5 mm nozzle, its storage duration was around 6 days less than
415 the 5 mm nozzle. One physical cause of this effect is the different shapes of both the ice structures. A flat
416 sheet of ice (effectively a cone with a high spray radius) with higher mass might have a storage duration
417 shorter than a conical ice structure. As the spray radius decreases with increasing nozzle diameter, the ice
418 structure's average slope increases and so the 5 mm nozzle's ice structure is "more" conical than the 3 mm
419 ice structure. Fig. 10 shows that a nozzle diameter of 3 mm has an average freeze rate ($3.2 \text{ l min}^{-1} \text{ w.e.}$)
420 which is large enough to increase the storage efficiency and small enough to not reduce the storage duration
421 of the Icestupa significantly.

7 CONCLUSIONS

422 We outlined a methodology for estimating ice, liquid water, water vapour and runoff quantities produced
423 during the construction of an Icestupa using measurements of fountain spray rate, air temperature, radiation,
424 humidity, pressure, wind and cloudiness at the EP study site. The comparison with validation measurements
425 at two different dates during the experiment led to satisfying results, although a more rigorous model
426 validation was not possible due to few icestupa volume measurements.

427 According to the model, the EP Icestupa achieved a storage quantity of 1392 litres of water with a
428 storage duration of 61 days. However, the corresponding storage efficiency was very low with only 7.5 %
429 for a water input of 18,584 litres. These estimates were most sensitive to the temperature threshold that
430 determined precipitation phase and ice emissivity parameters which created an uncertainty of $1.2 \pm 0.3 \text{ m}^3$
431 in the maximum ice volume calculated. This is to be expected as net longwave radiation and net shortwave
432 radiation together accounted for around 50 % of the overall energy turnover.

433 Although the location, storage quantity and duration of our experimental EP Icestupa are not representative
434 of the much larger Icestupas of Ladakh, the model results do support the hypothesis that there could be
435 considerable water loss during the formation of Icestupas particularly due to excessive fountain spray.
436 Using model calculations, it was shown that a decreased fountain nozzle diameter of 3 mm can increase the
437 storage efficiency drastically. This is because a change in the fountain nozzle diameter causes an effective
438 change of the ice surface area over which the net energy flux can act. This result has relevance on the future
439 design of Icestupa fountains. However, care has to be taken as our model is currently only validated by one
440 experiment at the EP site. Further experiments at different locations with different fountains are required to
441 better understand the influence of construction decisions on the results.

8 APPENDIX

442 8.1 Ladakh Icestupa 2014/15

443 A 20 m tall Icestupa (Wangchuk, 2015c) was built in Phyang village, Ladakh at an altitude of 3500
444 m a.s.l. Assuming a conical shape with a diameter of 20 m, the corresponding volume of this Icestupa
445 becomes 2093 m³ or 1,919,587 litres w.e. The fountain sprayed water at a rate of 210 l min⁻¹ (Wangchuk,
446 2015e) from 21st January (Wangchuk, 2015a) to at least until 5th March 2015 (Wangchuk, 2015b) (around
447 43 nights). Assuming fountain spray was active for 8 hours each night, we estimate water consumption to
448 be around 4,334,400 litres. So just during construction/freezing period of the Icestupa, roughly 56 % of the
449 water provided was wasted. The actual water loss is bound to be much higher due to further vapour losses
450 during the melting period. This Icestupa completely melted away on 6th July 2015 (Wangchuk, 2015d).
451 Therefore, the storage duration was 166 days or roughly 5 months.

CONFLICT OF INTEREST STATEMENT

452 The authors declare that the research was conducted in the absence of any commercial or financial
453 relationships that could be construed as a potential conflict of interest.

AUTHOR CONTRIBUTIONS

454 SB wrote the initial version of the manuscript. MH, ML, SW, JO, and FK commented on the initial
455 manuscript and helped improve it. SB developed the methodology with inputs from MH. SB performed the
456 analysis with support from MH and ML. SB and MH participated in the fieldwork.

FUNDING

457 This work was supported and funded by the University of Fribourg and by the Swiss Government Excellence
458 Scholarship (Suryanarayanan Balasubramanian).

ACKNOWLEDGMENTS

459 We thank Mr. Adolf Kaeser and Mr. Flavio Catillaz at Eispalast Schwarzsee for their active participation
460 in the fieldwork. We would also like to thank Digmesa AG for subsidising their flowmeter used in the
461 experiment. We would particularly like to thank the editor Prof. Thomas Schuler who gave us important
462 inputs to improve the paper and we thank also Prof. Christian Hauck and Prof. Nanna B. Karlsson for
463 valuable suggestions that improved the manuscript.

DATA AVAILABILITY STATEMENT

464 The data and code used to produce results and figures will be published at a later stage and can, until then,
465 be obtained from the authors upon request.

REFERENCES

- 466 Apel, H., Abdykerimova, Z., Agalhanova, M., Baimaganbetov, A., Gavrilenko, N., Gerlitz, L., et al. (2018).
467 Statistical forecast of seasonal discharge in central asia using observational records: development of a
468 generic linear modelling tool for operational water resource management. *Hydrology and Earth System*
469 *Sciences* 22, 2225–2254. doi:10.5194/hess-22-2225-2018
- 470 Bonales, L. J., Rodriguez, A. C., and Sanz, P. D. (2017). Thermal conductivity of ice prepared under
471 different conditions. *International Journal of Food Properties* 20, 610–619. doi:10.1080/10942912.
472 2017.1306551

- 473 Buck, A. L. (1981). New equations for computing vapor pressure and enhancement factor. *Journal of*
474 *Applied Meteorology and Climatology* 20, 1527 – 1532
- 475 Buytaert, W., Moulds, S., Acosta, L., Bievre, B. D., Olmos, C., Villacis, M., et al. (2017). Glacial melt
476 content of water use in the tropical andes. *Environmental Research Letters* 12, 114014. doi:10.1088/
477 1748-9326/aa926c
- 478 Chen, Y., Li, W., Deng, H., Fang, G., and Li, Z. (2016). Changes in central asia's water tower: Past, present
479 and future. *Nature* doi:10.1088/1748-9326/aa926c
- 480 Chevuturi, A., Dimri, A. P., and Thayyen, R. J. (2018). Climate change over leh (ladakh), india. *Theoretical*
481 *and Applied Climatology* 131, 531–545. doi:10.1007/s00704-016-1989-1
- 482 [Dataset] Copernicus Climate Change Service (C3S) (2017). Era5: Fifth generation of ecmwf atmospheric
483 reanalyses of the global climate
- 484 Cuffey, K. M. and Paterson, W. S. B. (2010). *The Physics Of Glaciers* (Elsevier)
- 485 Fujita, K. and Ageta, Y. (2000). Effect of summer accumulation on glacier mass balance on the
486 tibetan plateau revealed by mass-balance model. *Journal of Glaciology* 46, 244–252. doi:10.3189/
487 172756500781832945
- 488 Garratt, J. R. (1992). *The Atmospheric Boundary Layer* (Cambridge University Press)
- 489 Grossman, D. (2015). As himalayan glaciers melt, two towns face the fallout
- 490 Hock, R., Rasul, G., Adler, C., Cáceres, B., Gruber, S., Hirabayashi, Y., et al. (2019). 2019: High mountain
491 areas. *IPCC Special Report on the Ocean and Cryosphere in a Changing Climate* [H.-O. Pörtner, D.C.
492 Roberts, V. Masson-Delmotte, P. Zhai, M. Tignor, E. Poloczanska, K. Mintenbeck, A. Alegria, M. Nicolai,
493 A. Okem, J. Petzold, B. Rama, N.M. Weyer (eds.)]
- 494 Hoelzle, M., Barandun, M., Bolch, T., Fiddes, J., Gafurov, A., Muccione, V., et al. (2019). *The status and*
495 *role of the alpine cryosphere in Central Asia*. doi:10.4324/9780429436475-8
- 496 [Dataset] IDAWEB (2019). Meteoswiss, federal office of meteorology and climatology
- 497 Immerzeel, W. W., Lutz, A. F., Andrade, M., Bahl, A., Biemans, H., Bolch, T., et al. (2019). Importance
498 and vulnerability of the world's water towers. *Nature* 577, 364 – 369. doi:10.1038/s41586-019-1822-y
- 499 Meteoblue (2020). Climate schwarzsee
- 500 Mölg, T. and Hardy, D. R. (2004). Ablation and associated energy balance of a horizontal glacier surface
501 on kilimanjaro. *J. Geophys. Res.-Atmos.* 109, 1–13. doi:10.1029/2003JD004338
- 502 Nüsser, M., Dame, J., Kraus, B., Baghel, R., and Schmidt, S. (2019a). Socio-hydrology of artificial glaciers
503 in ladakh, india: assessing adaptive strategies in a changing cryosphere. *Regional Environmental Change*
504 doi:10.1007/s10113-018-1372-0
- 505 Nüsser, M., Dame, J., Parveen, S., Kraus, B., Baghel, R., and Schmidt, S. (2019b). Cryosphere-Fed
506 Irrigation Networks in the Northwestern Himalaya: Precarious Livelihoods and Adaptation Strategies
507 Under the Impact of Climate Change. *Mountain Research and Development* 39. doi:10.1659/
508 MRD-JOURNAL-D-18-00072.1
- 509 Oerlemans, J. and Knap, W. H. (1998). A 1 year record of global radiation and albedo in the
510 ablation zone of morteratschgletscher, switzerland. *Journal of Glaciology* 44, 231–238. doi:10.
511 3189/S0022143000002574
- 512 Scherrer, S. C. (2020). Temperature monitoring in mountain regions using reanalyses: lessons from the
513 alps. *Environmental Research Letters* 15, 044005. doi:10.1088/1748-9326/ab702d
- 514 Schmidt, L. S., Aðalgeirsdóttir, G., Guðmundsson, S., Langen, P. L., Pálsson, F., Mottram, R., et al. (2017).
515 The importance of accurate glacier albedo for estimates of surface mass balance on vatnajökull: evaluating
516 the surface energy budget in a regional climate model with automatic weather station observations. *The*
517 *Cryosphere* 11, 1665–1684. doi:10.5194/tc-11-1665-2017

- 518 Tetens, O. (1930). Über einige meteorologische begriffe. z. *Geophys.* 6, 297–309
- 519 Unger-Shayesteh, K., Vorogushyn, S., Farinotti, D., Gafurov, A., Duethmann, D., Mandychev, A., et al.
520 (2013). What do we know about past changes in the water cycle of central asian headwaters? a review.
521 *Global and Planetary Change* 110, 4 – 25. doi:10.1016/j.gloplacha.2013.02.004. Water in Central Asia
522 – Perspectives under global change
- 523 Wangchuk, S. (2014). Ice stupa artificial glaciers of ladakh
- 524 Wangchuk, S. (2015a). The good news at ice stupa 24th january 2015
- 525 Wangchuk, S. (2015b). Ice stupa artificial glacier inaugurated 5th of march 2015
- 526 Wangchuk, S. (2015c). Ice stupa surpasses guiness world record
- 527 Wangchuk, S. (2015d). Ice stupa way of celebrating a special day
- 528 Wangchuk, S. (2015e). World water day at ice stupa
- 529 WMO (2018). *Guide to Instruments and Methods of Observation* (World Meteorological Organization ;
530 2018 (2018 Edition))
- 531 Woolf, H. M. (1968). *On the Computation of Solar Elevation Angles and the determination of sunrise and*
532 *sunset times* (National Aeronautics and Space Administration)
- 533 Zhou, S., Kang, S., Gao, T., and Zhang, G. (2010). Response of zhadang glacier runoff in nam co basin,
534 tibet, to changes in air temperature and precipitation form. *Chinese Science Bulletin* 55, 2103–2110.
535 doi:10.1007/s11434-010-3290-5